



Modeling of Sachal Wind Project, Jhimpir and analysis of voltage regulation of the model with Sliding Mode Control-based Cuk Converter

Ramsha Manzoor Panhwar*, Asadullah, Aamir Sario, Amrat Punhuani, Ashfaque Ahmed Hashmani and Anwar Ali Sahito

Department of Electrical Engineering, Mehran University of Engineering & Technology, Jamshoro, Pakistan

*Corresponding author email: ramshapanhwar1975@gmail.com

ABSTRACT

Pakistan, rich in wind energy, currently incorporates 36 operational wind farms. Sachal Wind Project, Jhimpir, Sindh is a CPEC project having 33 wind turbines of 1.5MW each, cumulatively supplying 49.5 MW to the national grid. As wind speed is stochastic, it causes variations in the turbine voltage and its power generated. In the absence of a suitable mechanism that regulates the turbine voltage, wind turbines fail to supply the grid with rated power at a constant voltage. This is poor voltage regulation, and it deteriorates power quality and reliability. Turbine manufacturers employ power electronics DC-DC converters with Maximum Power Point Tracking (MPPT) control to maintain the voltage. Among the different DC-DC converters, the Cuk converter is an interesting topology. One of the simplest and most robust MPPT controls is Sliding Mode Control (SMC). This article is dedicated to developing a model of one of the 33 grid-connected turbines of Sachal Wind Farm on MATLAB Simulink using the system data and secondly, to addressing the problem of voltage regulation in the Wind Energy System (WES) using an SMC Cuk converter. A comprehensive design of each module of the WES is laid out. All modules are individually simulated and later integrated. The final 1.5MW Sachal Wind Farm model is analyzed under varying wind conditions. The simulation results show that rated power is delivered to the grid at rated voltage despite the wind variations, and the overall results of the model match with the system data validating the model design and performance.

Keywords:

Cuk converter, Sliding Mode Control, Sachal Wind Farm Jhimpir, Voltage regulation, WES and SMC

1. Introduction

Currently, wind energy is the most significant nonconventional renewable [1]. Apart from being the most rapidly growing renewable energy (RE) during the past twenty years [2], it is also the most economically advantageous RE in terms of capital cost, fuel cost, operation cost, projected utilization rate, and maintenance cost [3]. The power generation in Pakistan is a cumulative contribution from several public and private energy providers including GENCOS, WAPDA, IPPs, and K-Electric through various REs and non-REs [4]. Fig. 1 depicts the percent share of

all REs and non-REs employed for power generation in Pakistan in 2023. Currently, Pakistan has a total installed power generation capacity of 43,775 MW. At present, there are 36 operational private wind projects producing approximately 1335MW [5].

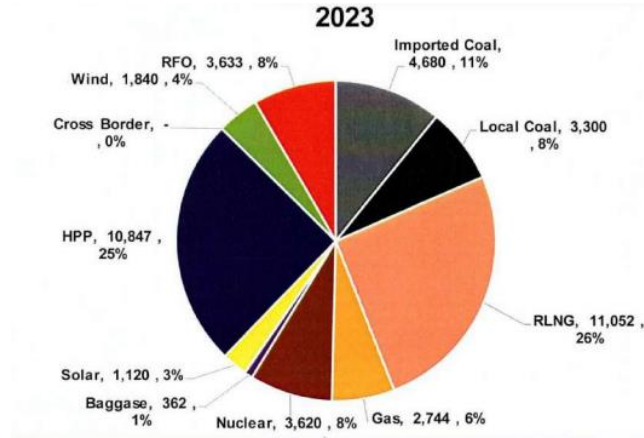


Fig. 1: Pakistan Net Power Generation Mix [4]

Sachal Wind Power Project, a subsidiary of Arif Habib Corporation Limited-one of the leading business groups of Pakistan, is a CPEC energy project located in Jhimpir in the Sindh province of Pakistan. The company employed the Chinese company Hydrochina Ltd. for engineering, procurement, construction, operation and maintenance services in April, 2012. The Industrial and Commercial Bank of China (ICBC) provided US \$ 107 million for the construction of this wind farm. Under Pak-China Economic Corridor (CPEC) projects, it is the first wind power project to achieve this breakthrough. It has a total of 33 installed Wind Turbine Generators (WTGs) of Goldwind company with a capacity of 1.5MW each and a voltage rating of 620V. So, the total installed capacity of the wind project is 49.5 MW [6].

The amplitude and frequency of the generated voltage of wind plants vary according to the speed of the wind [7]. Thus, power electronics interfaces are used to convert the generated voltage to a fixed DC voltage by means of active rectifiers and MPPT-controlled DC-DC converters, which can later be either stored or converted into required AC voltage and frequency using inverter circuits. A WECS can work in two separate modes - grid-connected and standalone mode. In this work, a grid-connected WECS of Sachal Wind Farm is modeled. When a small wind turbine unit is connected to the grid, the voltage and frequency at the point of common coupling are controlled by the grid. However, in the case of weak grids, voltage sags and disturbances do occur when the Wind Energy Conversion System (WECS) is interfaced to the grid. In such situations, the wind unit must support the grid voltage.

Authors in [8] have implemented a wavelet-based energy function for a 10 kW WECS to detect grid disturbances and to obtain a smooth transition between the two modes – grid-connected and standalone. To ensure good power quality, an LCL filter is employed to reduce ripples. Phase Lock Loop (PLL) is used for synchronization whenever the mode changes from standalone to grid-connected.

Some AI techniques such as fuzzy logic are also used in combination with DC-DC converters to regulate the voltage of Wind Turbine Generator (WTG). In like manner, the authors in [9] have modeled, analyzed, and built a prototype of a low-voltage fuzzy logic-controlled buck-boost converter module with a WTG. This work also takes account of several parameters of the WTG including torque, rpm range, armature resistance, inductance, blade specification and rotor dimensions. The performance of the hardware for the buck-boost converter has a 2.6s delay time, a 3.835s uptime, a peak time of 4.9s, a steady-time at 3.2 s and a steady-state error of 1.92%. In the simulation results, the delay time is 0.04 s, the uptime is 0.16 s, the steady-state at 0.16 s and the steady-state error at 1.07%.

Recently, some scholars have carried out excellent work on the application of several MPPT control methods for nanogrids and hybrid grids. Scholars of [10] used a Perturb and Observe (P&O) based DBR-Cuk converter for a 390V and 1990W DC nanogrid and analyzed the converter under grid-connected and islanded mode of operation. The simulation results show that the P&O Cuk converter is able to maintain good voltage regulation when the wind speed is changed from 8m/s to 10m/s at time instant t_1 and 10m/s to 8m/s at t_2 . However, P&O has a long convergence time for small perturbations and large oscillations with large perturbations.

[11] implements a novel cascade PID and SMC controller for a Cûk converter, as the electrical drive, for a 10kW Permanent Magnet Synchronous Generator (PMSG) into a variable speed WECS for microgeneration applications. The PID control for the outer loop and SMC for the inner loop remove the inverse peak and delay time and allow the system to achieve the maximum power point in less than 50ms and the system exhibits an efficiency of up to 92.9%.

In [12], a PI control-based Cuk converter is designed for a PMSG-based WECS. The performance of the converter, when variable wind speeds impact generator voltage, is observed. The PI controller is designed to maintain the output voltage of the Cuk converter at the desired value. Moreover, a new topology of CHB Multi-Level Inverter (MLI) is proposed in this work. It includes the advantages of the conventional CHB inverter and eliminates the disadvantage of requiring

separate DC sources. The output voltage of the MLI is regulated, as the input to the MLI is fed by the converter. The simulation results show that the designed PI voltage controller can maintain the DC link voltage at the desired value despite the ups and downs in wind speed. However, the major drawback of using bare PI control is that it often produces excessive overshoot to a step command. In the simulation results of [12], the output voltage of Cuk converter has an overshoot of about 50V and the output voltage of MLI has an overshoot of nearly 60V.

Since this work is based on real-time data of Sachal Wind Farm, Jhimpir. The different power and voltage levels of this project are used in this work and are tabulated in Table 1. This data was extracted from the personnel of the project during a site tour to Sachal Wind Project, Jhimpir and is also present in [13].

Table 1: System Data of Sachal Wind Project, Jhimpir, Thatta, Sindh, Pakistan

No.#	System Parameter Description	Value of Parameter
1.	Rated wind speed	3m/s
2.	RMS value of line-to-line output voltage of WTG	620V
3.	AC power generated by WTG	1.5MW
4.	DC fluctuating voltage after rectifier	600V
5.	DC voltage stable after DC-DC converter	600V
6.	Line-to-line RMS grid voltage	620V \pm 10%
7.	Average AC power delivered to the grid by single WTG	1.5MW
8.	Power factor	1
9.	Blade pitch angle	5°
10	Generator speed	1800 RPM

Fig. 2 gives the block diagram of the complete system modeled in this article. It represents an equivalent circuit of one of the 33 grid-connected WTG units installed in Sachal Wind Farm, Jhimpir. A comprehensive design of Cuk converter, three-phase active rectifier and three-phase Voltage Source Inverter (VSI) is carried out. An SMC controller is used to control the Cuk converter while two separate Synchronous Reference Frame- Phase Lock Loop controllers are employed for both the rectifier and inverter circuits. To smoothen out the ripples and reduce the harmonics in current at the DC stage and the AC grid side, an LCL filter is designed for the WECS specifications. The WTG is implemented using a turbine block and a Permanent Magnet

Synchronous Generator (PMSG). The grid is implemented using three-phase controlled voltage sources.

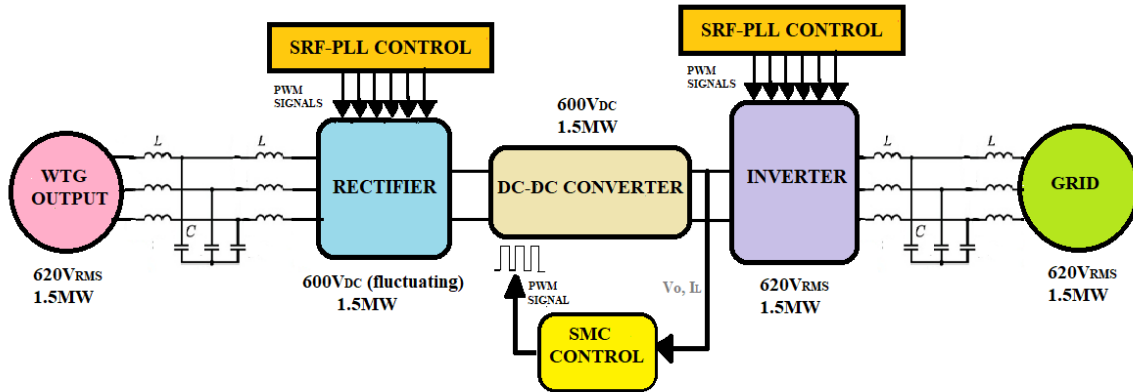


Fig. 2: Block diagram of the proposed model of Sachal Wind Farm, Jhimpir

Cuk Converter

The Cûk converter works by increasing or decreasing the voltage level by adjusting the duty cycle that controls the semiconductor switch of the circuit. This converter is used in electric vehicles and in power generation systems because it is dependable, has high efficiency, and has low harmonic production [13]. In the Cûk converter, the power does not flow directly from the source to the load; the storage energy elements take power from the source when the MOSFET switch is turned on and store the energy until the it turns off. Then the power flows from these storage elements to the load. The main energy-storage element is the capacitor C as shown in Fig. 3 also termed as the coupling capacitor. The significant function of the coupling capacitor C1 is to store energy and then transfer this energy to the load. The output voltage of Cuk converter is negative [14].

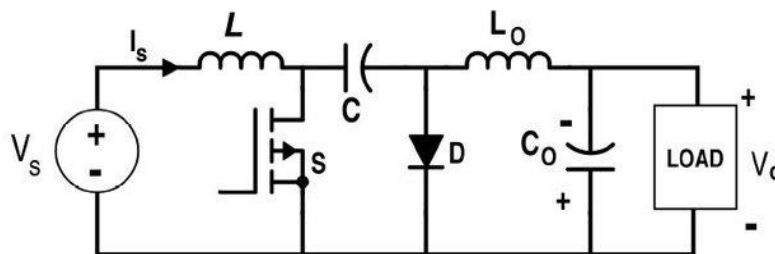


Fig. 3: Circuit diagram of Cuk converter [15]

Cuk converter has two different modes of operation. The first mode comes into play when the switch ‘S’ is in ON state and in the second mode the switch ‘S’ is in OFF state.

Mode 1:

When MOSFET is in ON state, inductor L_1 is directly connected to the input source. The voltage across L_1 is expressed in (1). Inductor L_2 is connected in series with C and the output capacitor. The voltage across L_2 is expressed in (2).

$$V_{L1} = V_s \tag{1}$$

$$V_{L2} = V_o + V_{C2} \tag{2}$$

The resulting circuit of Cuk converter in mode 1 is depicted in Fig. 4.

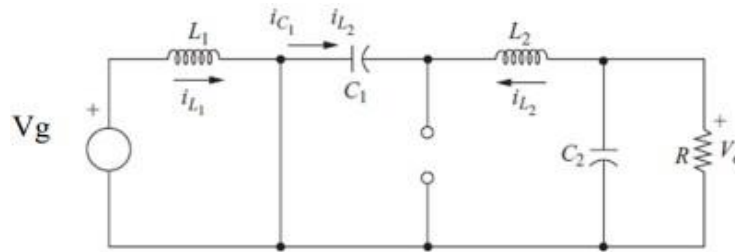


Fig. 4: Equivalent circuit of Cuk converter in mode 1 [15]

Mode 2:

In mode 2, the MOSFET 'S' is in OFF state. In the OFF state, diode D is forward biased, Inductor L_1 is directly connected in series with the source V_s and the coupling capacitor C_1 . The voltage across L_1 is expressed in (3). While L_2 is directly connected to the output capacitor. The voltage across L_2 is expressed in (4).

$$V_{L1} = V_s - V_{C1} \tag{3}$$

$$V_o = V_{L2} \tag{4}$$

The resulting circuit of Cuk converter in mode 2 is given in Fig. 5.

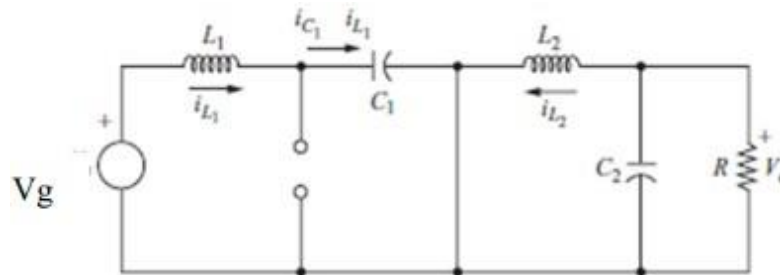


Fig. 5: Equivalent circuit of Cuk converter in mode 2 [15]

Sliding Mode Controller for Cuk Converter

Power electronic converters cannot withstand large inductor currents for two reasons: it can cause the inductor core to saturate with consequent even high peak current value or can be simply greater than the maximum allowed switch current [17]. Therefore, it is necessary to introduce a protection into the controller that prevents the inductor current from reaching dangerously high values. The hysteresis loop provides this protection. The linear voltage control, on the other hand, improves the voltage regulation [17]. The control circuit of SMC comprises of two control loops as shown in Fig. 6. The outer voltage control loop is implemented by a combination of proportional and integral control. The inner main current loop is represented by hysteresis control block which is also known as relay block. The control circuit of SMC is shown in Fig. 6. The two combined loops form the SMC as a whole.

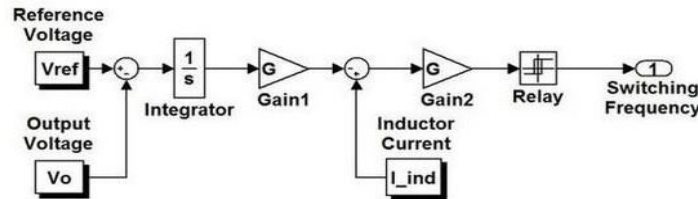


Fig. 6: Control Circuit of Sliding Mode Controller [17]

The K_p and K_i gains of the PI controller in the proposed SMC are tuned using the hit and trial technique [18]. They are given in Table. 4. The selected ON and OFF time of the hysteresis controller along with the respective outputs are also given Table. 4.

An SMC Cuk converter can be implemented by first setting a constant output reference voltage. This reference voltage is compared with the actual output of the Cuk converter. This comparison leads to an error. The resulting error is given to the PI controller of the SMC which generates reference inductor current. Both the reference current and actual input inductor current are compared. The resulting error is given to Hysteresis controller of SMC which generates appropriate pulse width modulated signal for the MOSFET switch of the converter. The connections block diagram of SMC with the DC-DC converter is given in Fig. 7.

LCL Filters

LCL filters are specially designed to reduce the harmonics of current absorbed by power converters, with a rectifier at the input stage and an inverter at the output stage. LCL filter is a parallel-series combination of inductors and capacitors used to reduce the harmonic content of the output voltages and currents of rectifiers and inverters [19]. The LCL filter effectively smooths the output currents of the three-phase active rectifier and the three-phase voltage source inverter, and supplies the filtered harmonic-free current from the grid and to the grid, respectively.

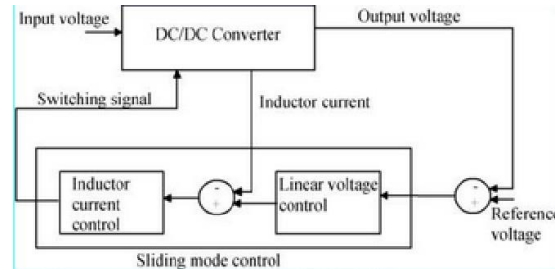


Fig. 7: Connections block diagram of SMC with DC-DC converter [17]

Grid currents are not purely sinusoidal as they contain harmonics. These non-sinusoidal currents cause power quality issues. LCL filter removes this complexity by filtering out all the harmonics and delivering purely sinusoidal currents. The advantages of LCL filters are superior performance than the other filters, high attenuation, improved performance, cost-effectiveness, and less weight and size [20].

Clarke's Transformation

The Clarke's transformation converts the time domain components of a three-phase system which are given in abc frame into two components in an orthogonal stationary frame ($\alpha\beta$) [21]. Fig. 8 illustrates the Clarke's transformation.

Park's Transformation

Park's transformation represents the sinusoidal currents obtained from Clarke's transformation into DC quantities on an orthogonal dq frame, rotating synchronously at the detected grid fundamental frequency [22]. Park transformation is indicated in Fig. 9.

In grid-following converters, the reference currents i_d^* and i_q^* are usually provided by a power controller, which regulates the active and reactive power delivered to the grid [22].

Direct Quadrature (dq) Control

Direct Quadrature (dq) control, also called Synchronous Reference Frame (SRF) control, is a current control technique based on a reference frame transformation module for transforming the current and voltage parameters of the utility grid to a reference frame that rotates synchronously.

This transformation is done by first using Clarke transformation and then the Park transformation methods, which convert the abc to $\alpha\beta$ and $\alpha\beta$ to dq respectively. In dq -control, PI controllers are extensively used owing to their capability of regulating the DC signals without steady-state error [23]. Fig. 10 shows the schematic of the implementation of dq -control in a grid-connected system.

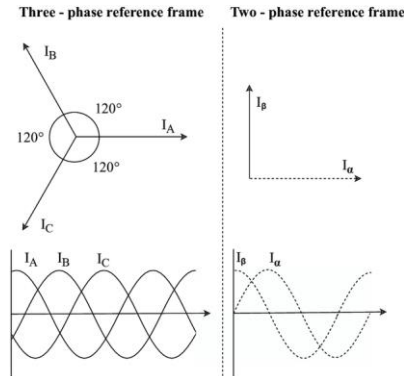


Fig. 8: Graphical representation of Clarke's transformation [21]

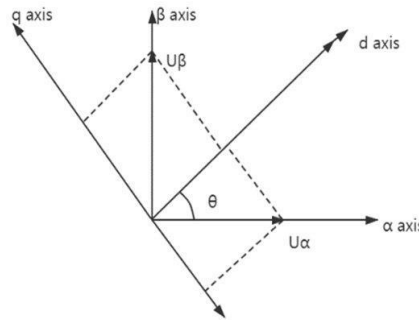


Fig. 9: Graphical representation of Park's Transformation [22]

Phase Lock Loop (PLL) Algorithm

In the proposed system, PLL is used to generate the signal which is used as the reference for the implementation of current controller in the grid connected inverter and rectifier circuit. The PLL algorithm is used to detect the phase angle and the frequency of the input voltage, and then the reference current is generated [24]. In the DQ-PLL control system, the grid voltage has two components that is direct voltage component 'Vd' and quadrature voltage component 'Vq' as shown in phasor diagram in Fig. 11.

To send active current to the grid, the reference current signal should be in phase with the actual voltage. The reference quadrature voltage component is set to zero to make the 'Vq' zero as indicated in phasor diagram in Fig. 12. Thus, 'Vd' is in phase with the actual voltage.

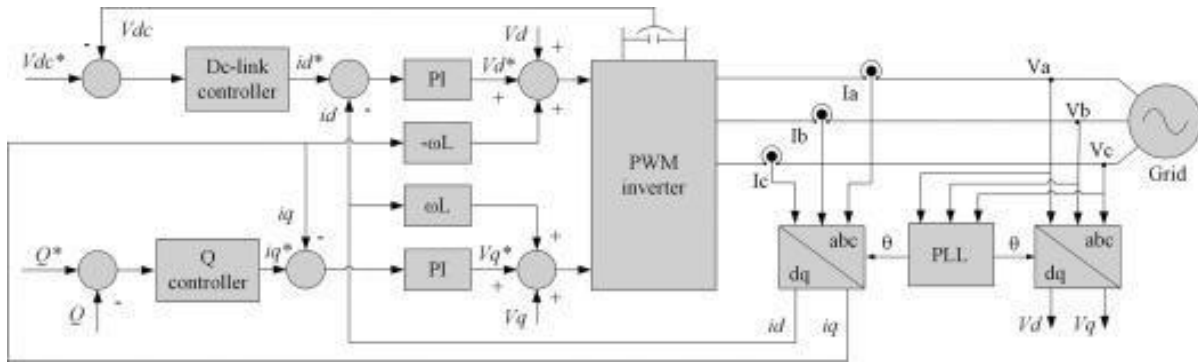


Fig. 10: Implementation of dq-Control in a Grid-Connected System [23]

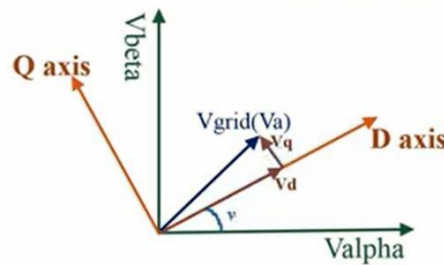


Fig. 11: Grid voltage ‘Vg’ and its components ‘Vd’ and ‘Vq’ in DQ and $\alpha\beta$ frame [24]

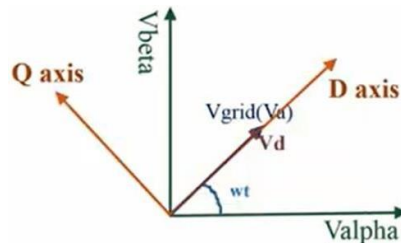


Fig. 12: Phasor diagram of ‘Vg’ in DQ and $\alpha\beta$ frame when $V_q=0$ and ‘Vd’ is in phase with ‘Vg’ [24]

Fig. 13 depicts the implementation of PLL algorithm with DQ control structure. Clarke and Park transformation is employed to transform three phase voltages into two phase $\alpha\beta$ voltage components and then to convert them into DQ components.

“ ωt ” is the angle between the alpha voltage component ‘ V_α ’ and the direct voltage component ‘Vd’. The integrator block in PLL control algorithm in Fig. 13 is responsible for adjusting the “ ωt ” angle to obtain the condition of active current signal generation when ‘ V_{qref} ’ is set to zero.

The active component is aligned in phase with alpha and the reactive component is aligned in phase with beta component.

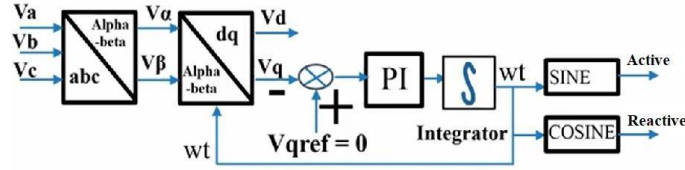


Fig. 13: Implementation of PLL algorithm

2. Methods

2.1. Design of Open Loop Cuk Converter as per System Data

A 5% variation has been assumed in the input voltage of the Cuk converter in both buck and boost mode with respect to the output. These supply variations will account for the variation in wind speed. The resulting input voltages in both modes and other design parameters of the Cuk converter are indicated in Table 2.

There are mainly four design elements in a Cuk converter. They are L1, L2, C1 and C2. Before the computation of these parameters, the DC input supply 'Vin' along with its frequency and DC output requirement 'Vo' must be known [14]. Then, duty cycle 'D' is calculated using Eq. 5

$$M_V = \frac{V_o}{V_{in}} = - \left(\frac{D}{1-D} \right) \quad (5)$$

Input inductor L1 current is determined using Eq. 6:

$$I_{L1} = \frac{P_{in}}{V_{in}} \quad (6)$$

Output inductor L2 current can be computed using (7):

$$I_{L2} = \frac{P_o}{V_o} \quad (7)$$

The load resistance R can be found using Eq. 8:

$$R = \frac{V_o^2}{P_o} \quad (8)$$

Input inductance value can be determined by Eq. 9:

$$L_1 = \frac{D.V_o}{\Delta I_{L1}.f} \quad (9)$$

Output inductance value can be determined by 10:

$$L_2 = \frac{D.V_o}{\Delta I_{L2}.f} \quad (10)$$

Input capacitance C1 value can be determined using Eq. 11:

$$C_1 = \frac{(1-D)V_o}{8L_2.R.f^2.\Delta V_{c1}} \quad (11)$$

Output filter capacitor C2 value can be found by Eq. 12:

$$C_2 = \frac{D}{R.(\frac{\Delta V_o}{V_{in}}).f} \quad (12)$$

Table 2: Selected Design Parameters for Open Loop Cuk Converter

S. No	Description	Value
1	Input voltage in boost mode with 5% variation	570V
2	Input voltage in buck mode with 5% variation	630V
3	Output voltage	600V
4	Switching frequency for MOSFET switch	50kHz
5	Power input	1.5MW
6	Power output	1.5MW
7	Allowable percent ripple in the inductor currents	10%
8	Allowable percent ripple in the input capacitor voltage	1%

Now using the relations above the duty cycle D can be calculated using Eq. 5 for both buck mode and boost as follows:

$$-\left(\frac{-600}{570}\right) = -\left(\frac{D}{1-D}\right)$$

Therefore, D=51.21% (for boost mode)

$$-\left(\frac{-600}{630}\right) = -\left(\frac{D}{1-D}\right)$$

Or D=100-54.04 = 48.7% (for buck mode)

The load resistance R can be found using Eq. 8:

$$R = \frac{600^2}{1500000}$$

$$R = 0.24\Omega$$

The inductor current I_{L1} and inductor current I_{L2} can be found using (6) and (7) respectively:

$$I_{L1} = \frac{1500000}{570}$$

$$I_{L1} = 2631.57A$$

$$I_{L1} = \frac{1500000}{600}$$

$$I_{L2} = 2500A$$

The ripple current for both inductors L1 and L2 of the Cuk converter should lie between 10%-30% astaken in Eq. 13 and Eq. 14. This is done to achieve a good compromise between inductor and capacitor size [14].

$$\Delta I_{L1} = 0.1 \times I_{L1} \quad (13)$$

$$\Delta I_{L2} = 0.1 \times I_{L2} \quad (14)$$

$$\Delta I_{L1} = 0.1 \times 2631.57$$

$$\Delta I_{L1} = 263.157A$$

$$\Delta I_{L2} = 0.1 \times 2500$$

$$\Delta I_{L2} = 250A$$

The maximum allowable ripple voltage for the output of a capacitor is 5% of the rated DC capacitor voltage [14]. A 1% ripple has been chosen for the output capacitor C2. Thus, the ripple voltage for C2 can be found using Eq. 15:

$$\Delta V_{C1} = 0.01(V_s - V_o) \quad (15)$$

$$\Delta V_{C1} = 0.01(600 - (-570))$$

$$\Delta V_{C1} = 11.7V$$

The parameters L1, L2, C1 and C2 are calculated using the equations (9), (10), (11) and (12). All the calculated parameters are listed in Table.3 and Table 4 enlists the parameters for SMC.

2.2. Design of LCL Filter for Rectifier and Inverter circuits

The LCL filter for both the rectifier and inverter will be the same. As given in the system data in Table.1, the phase-phase RMS value of the three-phase AC output voltage of WTG is 620V which is rectified into 600V by the rectifier. Also, the DC input for the inverter is 600V which is converted into three-phase AC voltage with phase-phase RMS value of 620V. The power input at the rectifier and the power output at the inverter is 1.5MW for both stages. Therefore, the same LCL filter will be employed for both the rectifier and the inverter.

In this work, the WTG will be modelled with an ideal three-phase sinusoidal voltage source having three-phases e_a , e_b and e_c and a fundamental frequency 'f'. Fig. 14 shows the connections of LCL filter with the three-phase output of the WTG and the three-phase active rectifier. The parameters L at the turbine side and the converter side represent filter inductor, while the parameter C represents the filter capacitor.

Table.3 Calculated Design Parameters of Open Loop Cuk Converter

S.No	Design Parameter	Value
1	L1	21.4988 μ H
2	L2	23.38 μ H
3	C1	2.1914mF
4	C2	104.19 μ F

Table. 4 Selected Parameters of Proposed SMC

S.No:	Parameter Description	Parameter Value
1	Kp for linear voltage controller	5
2	Ki for linear voltage controller	10000
3	Switch ON point for hysteresis controller	1
4	Switch OFF point for hysteresis controller	-1
5	Output of hysteresis controller during ON time	1
6	Output of hysteresis controller during OFF time	0

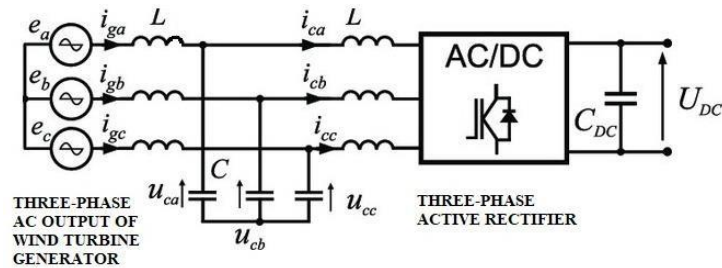


Fig. 14: LCL Filter Connections with WTG and Three-Phase Active Rectifier

Likewise, the same rating LCL filter will also be connected after the inverter stage as shown in Fig. 15. The grid is represented with an ideal three-phase voltage source with a fundamental frequency ‘f’ and the phases ‘e_a’, ‘e_b’ and ‘e_c’.

The transfer function between the grid current and inverter voltage can be determined by taking in account the equivalent per phase LCL filter circuit in the s-domain [20]. Fig. 16 shows the equivalent per phase LCL filter circuit in the s-domain. “V_i” is input voltage for the filter and “I_g” is the grid current.

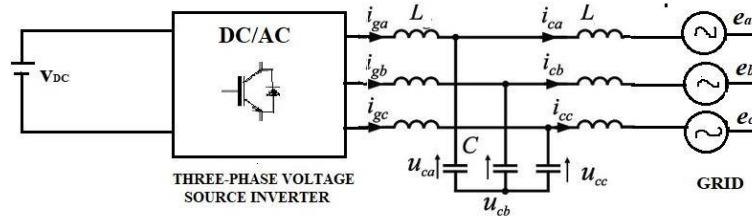


Fig. 15: LCL Filter connections with VSI and the Grid

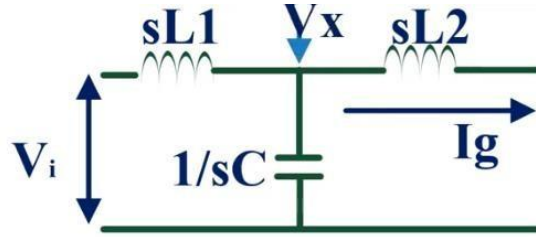


Fig. 16: Equivalent per phase LCL filter circuit in the s-domain

Applying KCL at point ‘x’:

$$\frac{V_i - V_x}{sL1} = -I_g + \frac{V_x}{\frac{1}{sC}} \quad (16)$$

‘V_x’ can be computed by Eq. 17:

$$V_x = I_g \cdot s \cdot L_2 \quad (17)$$

Solving Eqs. 16 and 17, Eq. 18 is obtained:

$$\frac{I_g}{V_i} = \frac{1}{L1L2Cs^3 + s(L1+L2)} \quad (18)$$

Substituting $L1+L2 = L$ and $Lp = \frac{L1L2}{L1+L2}$ in Eq. 18:

$$\frac{I_g}{V_i} = \frac{1}{sL(1+s^2CLp)} \quad (19)$$

Eq. (19) is the transfer function of the LCL filter of the system. The expression of resonant frequency ω_{res} is derived from Eq. 19 and given in Eq. 20:

$$\omega_{res} = \frac{1}{\sqrt{CLp}} \quad (20)$$

Table.5 contains the selected design parameters of LCL filter. The selection of resonant frequency should be as such that it is neither near to the fundamental frequency nor near to the switching frequency. As a rule of thumb, the resonant frequency should be 1/10th of the switching frequency [20]. The RMS voltage and the apparent power selected is as per the system data given

in Table.1 in section 2. Also, from section 2 Table.1, the power factor of the system is unity. So, the total apparent power of the system is equal to the active power.

Table.5 Selected Design Parameters of LCL Filter

S.No	Selected Parameters	Value
1.	Switching frequency	10kHz
2.	Resonant frequency	1000Hz
3.	Fundamental frequency	50Hz
4.	Apparent power	1.5MVA
5.	RMS voltage	620V

The expression for the capacitance of LCL filter is present in [20] and given below in Eq. 21.

$$C = \frac{0.05S}{2\pi fV^2} \quad (21)$$

Using (21), the value of C for the LCL filter is computed below:

$$C = \frac{0.05 \times \frac{1500000}{3}}{2\pi \times 50 \times 620^2}$$

$$C = 207.0173 \mu\text{F}$$

Using relation (20) in (19), the transfer function can be re-defined in Eq. 22:

$$\frac{I_g}{V_i} = - \frac{1}{sL(1 + \frac{s^2}{wres^2})} \quad (22)$$

At switching frequency $s = j\omega_{sw}$:

$$\frac{I_g(sw)}{V_i(sw)} = - \frac{1}{jwswL(1 + \frac{jwsw^2}{wres^2})} \quad (23)$$

Since $j^2 = -1$, the magnitude of (23) is given in Eq. 24:

$$\frac{I_g(sw)}{V_i(sw)} = \frac{1}{wswL(1 - \frac{wsw^2}{wres^2})} \quad (24)$$

From (24), the expression for L is given in (25):

$$L = \frac{1}{wsw \frac{I_g(sw)}{V_i(sw)} (1 - \frac{wsw^2}{w^2})} \quad (25)$$

The grid current 'I_g' can be calculated using Eq. 26:

$$I_g = \frac{S}{V_{rms}} \quad (26)$$

From Table.5 putting the values of 'S' and 'V_{rms}' in (26) the grid current is given in Eq. 27:

$$I_g = \frac{1500000}{620}$$

$$I_g = 806.451A \quad (27)$$

According to International Electrotechnical Commission (IEC) standard, the value of grid current at switching frequency must be equal to 0.3% of the grid current as given in Eq. 28:

$$I_{g(sw)} = 0.003I_g \quad (28)$$

$$I_{g(sw)} = 0.003 \times 806.451$$

$$I_{g(sw)} = 2.419A$$

For a sine triangular PWM scheme, the minimum value of 'Vi' at switching frequency is given in (29):

$$V_{i(sw)} = 0.9V_g \quad (29)$$

$$V_{i(sw)} = 0.9 \times 620$$

$$V_{i(sw)} = 558V \quad (30)$$

Substituting the values from (27) and (30) in (25):

$$L = 37.0837 \mu H \quad (31)$$

$$L_1 = L_2 = \frac{L}{2}$$

$$L_1 = L_2 = 18.54185 \mu H \quad (32)$$

(32) gives the minimum values of the inductances. The maximum values can be calculated using (33). It depends on the voltage drop across the inductance which is 20% of the grid voltage 'V_g':

$$L_{max} = \frac{0.2V_g}{2\pi f I_g} \quad (33)$$

Substituting values of 'I_g' and "V_g" in (33):

$$L_{max} = 489.43\mu H$$

$$L = L_1 = L_2 = \frac{L_{max}}{2}$$

$$L = \frac{489.43}{2}$$

$$L = 244.7168\mu H$$

Hence, the calculated L and C values for the LCL filter are given in Table.6.

Table.6 Calculated Parameters for LCL Filter

S.No	Parameter Description	Parameter Value
1.	Inductor L	244.7168μH
2.	Capacitor C	207.0173μF

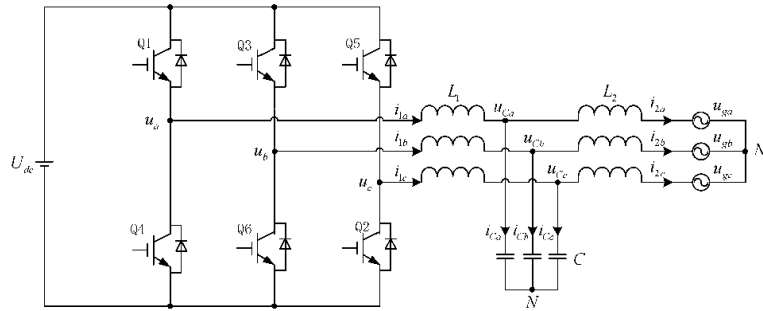


Fig. 17: Three-Phase Voltage Source Inverter (VSI) interconnected with Grid through LCL Filter [25]

The 6 IGBT switches require a gate pulse for each. In this work, these controlled gate pulses will be provided by the DQ controller. The grid is represented with a three-phase AC source and an LCL filter is employed to smooth out the harmonics in the inverter output current. A three-phase VSI converts a DC input voltage into a three-phase AC output. Thus, in the proposed system the output of the closed loop Cuk converter will serve as an input for the three-phase inverter. VSI converts that DC voltage into three-phase AC voltage and then it is transmitted to electricity grid.

A Sine PWM scheme with unipolar switching is used for PWM generation for all six IGBTs of the inverter [14]. The gate pulse of the two IGBTs of each leg of the VSI are opposite to each other. To implement this logic a NOT gate is placed with every alternate IGBT. The input reference voltages ‘ $V_{a\text{ref}}$ ’, ‘ $V_{b\text{ref}}$ ’ and ‘ $V_{c\text{ref}}$ ’ are generated by the DQ control.

The three-phase inverter for the system is implemented with DQ-control as explained in section 7.3 and 7.4. The general block diagram of grid-connected three-phase inverter with DQ-control is shown in Fig. 18.

For the proposed system, the DC bus voltage is maintained at 600V which is the output of the SMC Cuk converter. Thus, the input DC source for the inverter is chosen as 600V. A three-phase inverter bridge is made using IGBTs. An LCL filter is connected to filter out the harmonics in the grid current. The filter values L and C are set as calculated in section 6.2 and tabulated in Table. 6. The grid is represented by a three-phase source with line-to-line RMS voltage 620V and a fundamental frequency 50Hz.

To implement the dq-controller, the line-to-line voltages of the grid side need to be sensed. The three-phase voltages are transformed into two-phase alpha-beta voltages by Clarke’s transformation. Using these alpha-beta voltages PLL is implemented. Alpha beta voltages are

then converted to dq voltages using Park's transformation. The current 'id' corresponds to active current and 'iq' corresponds to reactive current. 'id' and 'iq' is then subtracted from the reference current to find the error. Error is fed to a PI controller to find voltages 'Ud' and 'Uq'. The PI gains for dq-current control loops and PLL control loops are set using hit and trial technique [18]. The PI gains are given in Table.7.

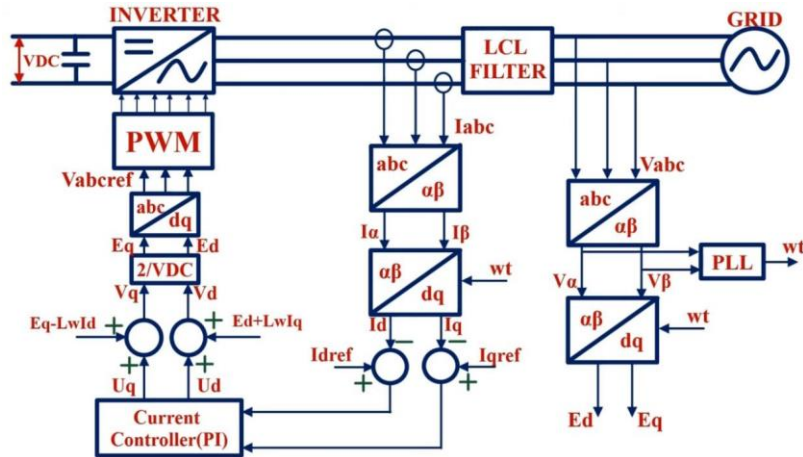


Fig. 18: Block diagram of grid-connected three-phase inverter with DQ-control and LCL filter [26]

Table. 7 Selected gains for PI controllers of DQ-controller and PLL

No.	Gain Parameter	Gain Value
1	Proportional gain "P" for 'Id' and 'Iq' current control loops	5
2	Integral gain "I" for 'Id' and 'Iq' current control loops	5000
3	Proportional gain "P" for PLL controller	10
4	Integral gain "I" for PLL controller	50000

'Ud' is then added with $E_d + L\omega i_q$ to get V_d , where ω is the grid frequency that is 50Hz and L is the filter inductor as computed in section 6.2. Similarly, U_q is added with $E_q - L\omega i_d$ to get V_q . Then V_d and V_q are multiplied with $2/V_{dc}$ to obtain 'Ed' and 'Eq'. They are then transformed into three-phase voltages to get the reference voltages for Pulse Width Modulated (PWM) signals for the SPWM controller. The three-phase active rectifier for the system is implemented with dq-control and PLL. The general block diagram of grid-connected three-phase rectifier with dq-control is shown in Fig. 19.

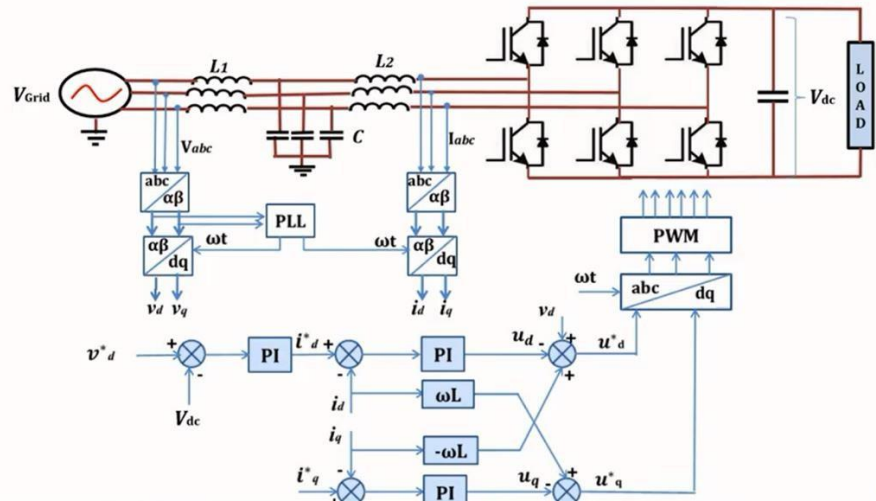


Fig. 19: Block diagram of grid-connected active rectifier with dq-control and LCL filter

In this work, the WTG implemented with a wind turbine block and coupled with a PMSG block. As tabulated in Table.1, the power generated by the Goldwind WTG is 1.5MW at 620V. A constant block is used to input the wind speed of 3m/s. A three-phase rectifier is made using 6 IGBTs. As used in the design of the three-phase inverter, a sine PWM scheme with unipolar switching is used for PWM generation for all six IGBTs of the rectifier.

The same LCL filter is employed for the rectifier. The dq- control structure is enhanced with a PI control block for the DC output voltage. The PI gains for this DC voltage PI block are set using the hit and trial technique and are given in Table. 8. The remaining gains of PI blocks are same as that of the inverter

Table. 8 Selected PI gains for DC voltage PI control block

No.	Gain Parameter	Gain Value
1	Proportional gain “P”	0.5
2	Integral gain “I”	200

3. Results and Discussion

Fig. 20 shows the complete integrated wind power system with SMC Cuk converter as designed in chapter 5, the LCL filter as designed in section 6.2, the grid-connected inverter as designed chapter 8 and the active rectifier as designed in chapter 9.

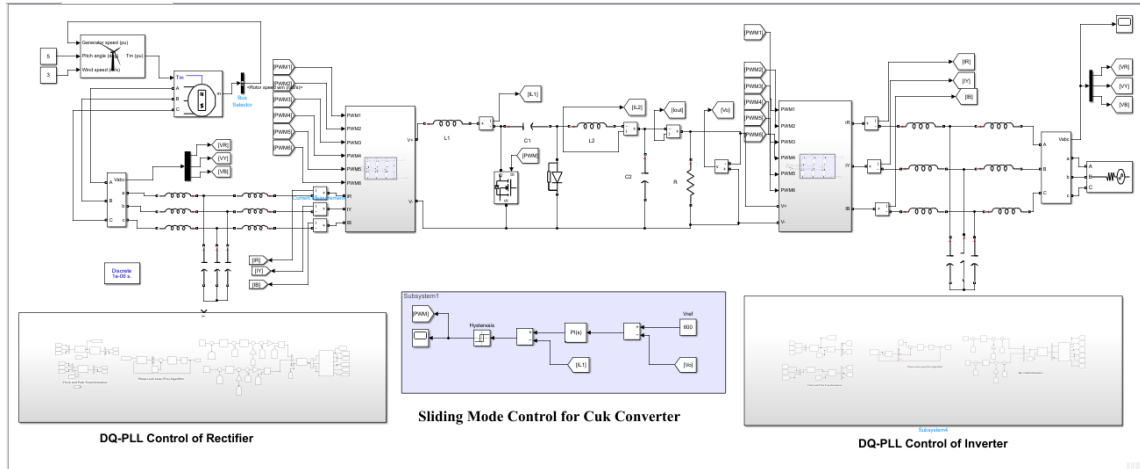


Fig. 20: Complete Integrated System MATLAB Simulink Model

Fig. 21 (a), (b) and (c) give the simulation results of the open loop Cuk converter designed in section 3.4 as per the system data in Table. 1. These results are ideal as these do not account for the variations in the wind speed. The output voltage is 600V as shown in Fig. 21 (a) which is as per system data in Table. 1. The input and output powers in Fig. 21(b) are at 1.5MW as in Table. 1. The input inductor L_1 current I_{L1} in Fig. 21(c) is 2600A as calculated in section 3.4 . The inductor L_2 current I_{L2} as well as output current I_o are both at 2500A as in section 3.4. The oscillations observed in all curves is due to the absence of a controller.

3.1. Simulation Results of the Proposed System at Rated Wind Speed

In this section, the simulation results of the each and every stage of the system at rated speed are presented. As seen in Fig. 22 (a), the wind speed is constant at 3m/s. Figs. 22 (b), (c) and (d) present the WTG voltage, power and current respectively. Fig. 23 (a) shows the input and output voltage of Cuk converter. The input voltage is the output of the rectifier plotted with blue while the pink curve indicates the output of the converter at rated speed. Figs. 23 (b) and (c) give the currents and power input and output of the converter respectively. Due to the addition of SMC, the oscillations in the output voltage, inductor currents and powers are greatly reduced compared to Figs. 22 (a), (b) and (c).

Figs. 24(a), (b) and (c) give the grid voltage, grid currents and power to delivered to the grid when wind speed is maintained at rated speed 3m/s.

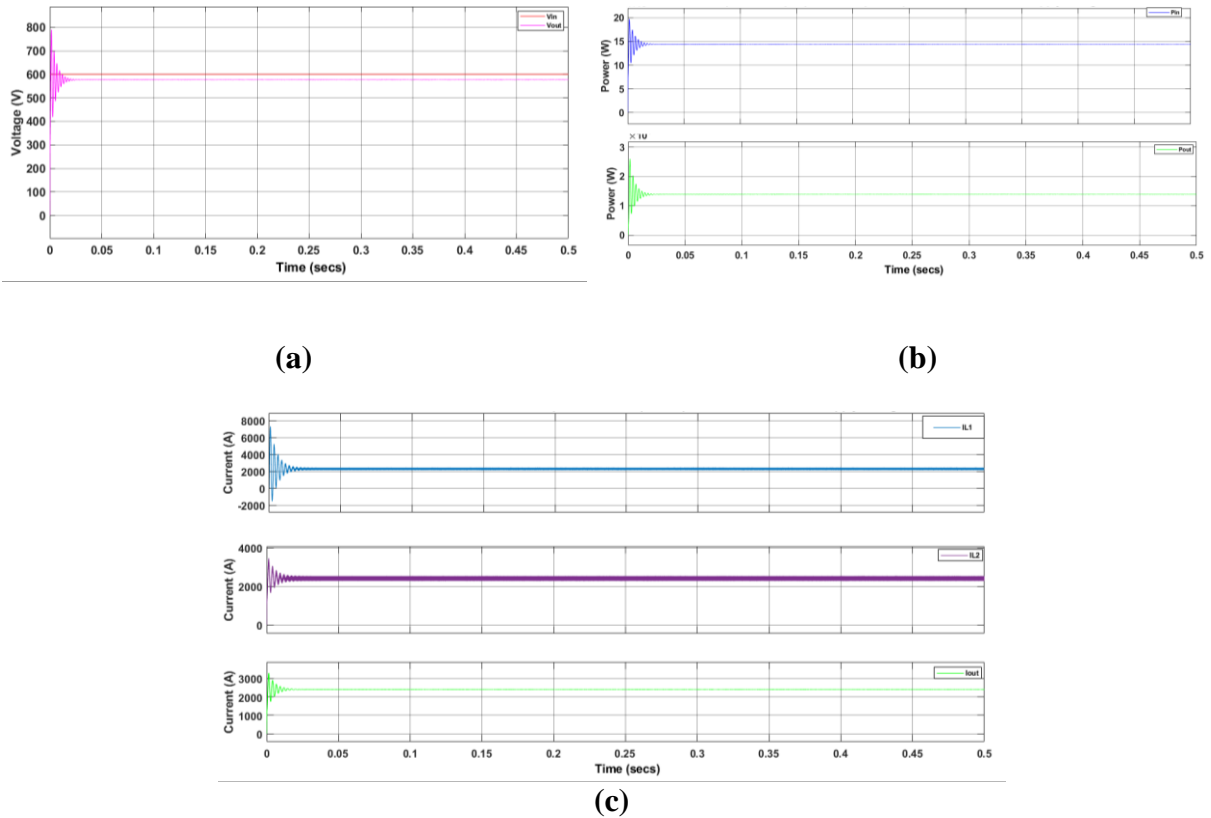


Fig. 21: (a) Output voltage of open loop Cuk converter (b) Input and output powers of open loop Cuk converter (c) Inductor L1 and L2 currents and output current of open loop Cuk converter

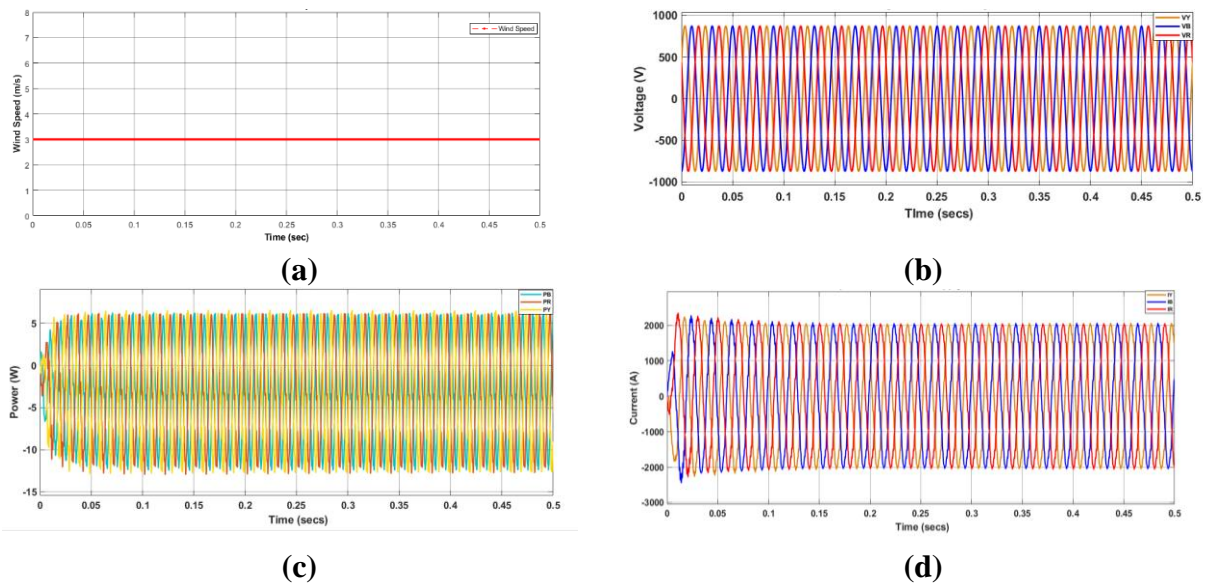


Fig. 22: (a) Wind profile (b) WTG three-phase voltage at rated wind speed (c) WTG three-phase power at rated wind speed (d) WTG three-phase current at rated wind speed

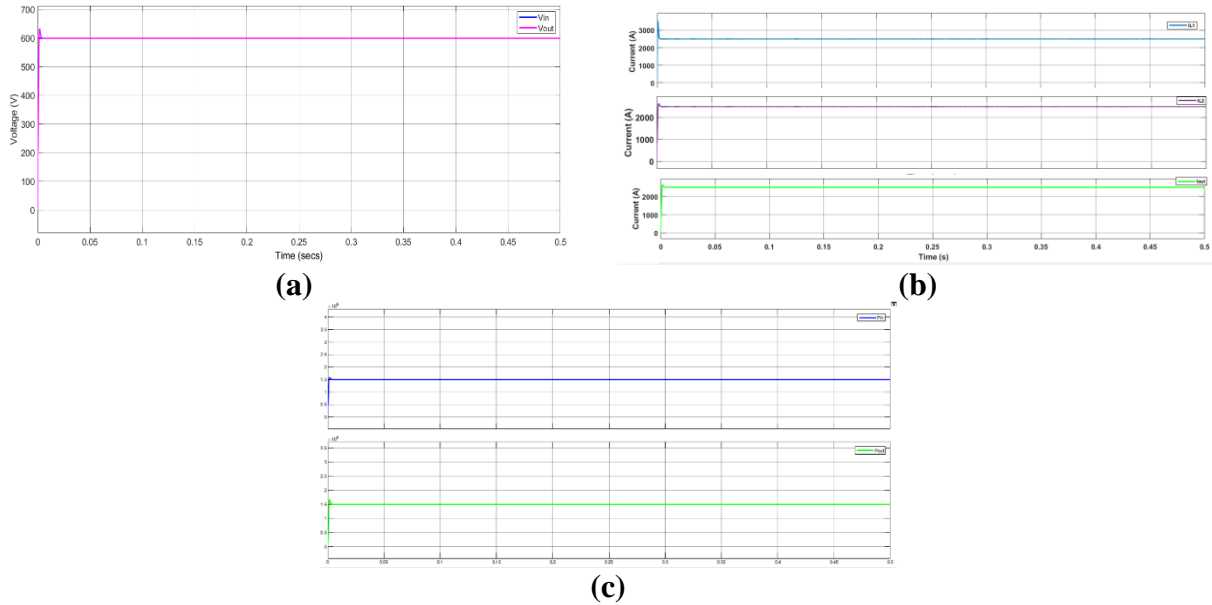


Fig. 23: (a) Output voltage of SMC Cuk converter at rated wind speed (b) Inductor L1 and L2 currents and output current of SMC Cuk converter at rated wind speed (c) Input and output powers of SMC Cuk converter at rated wind speed

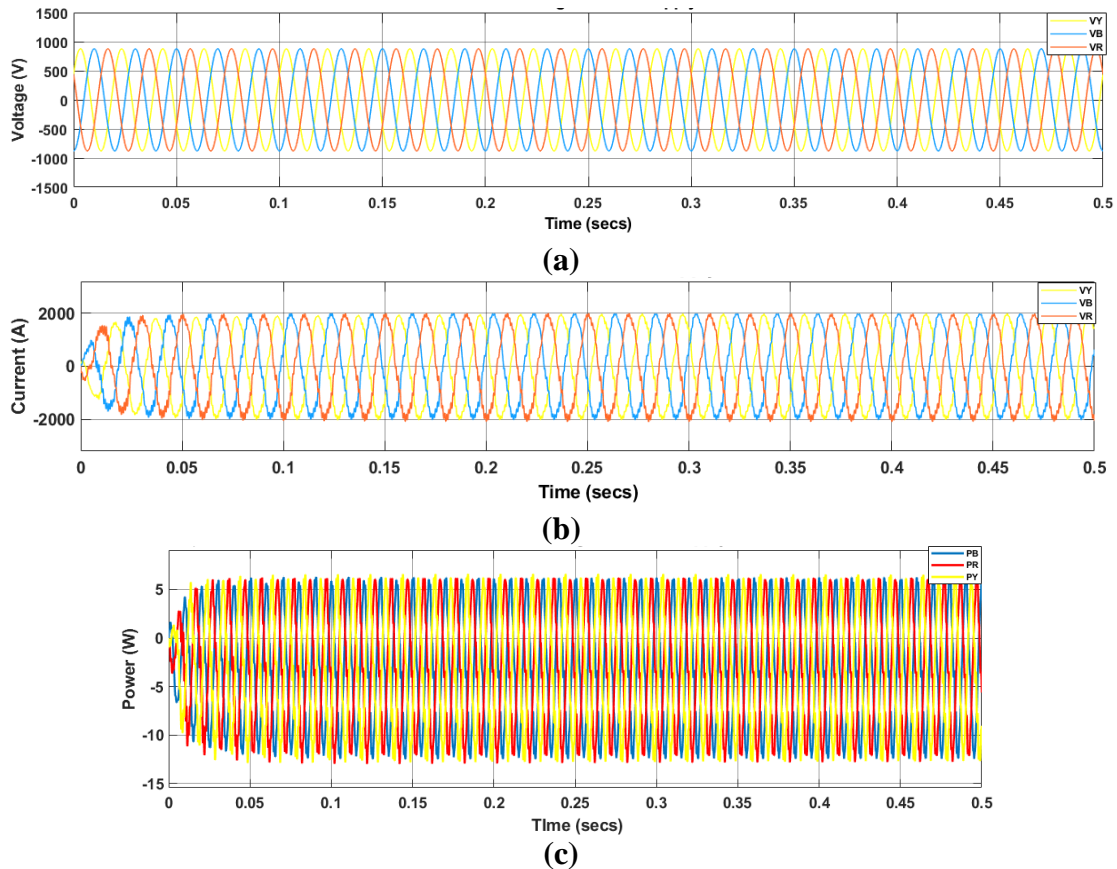


Fig. 24: (a) Grid voltage at rated wind speed (b) Grid current at rated wind speed (c) Power delivered to the grid at rated wind speed

According to the system data in Table. 1, at wind speed of 3m/s the Goldwind WTG of the system generates its rated power 1.5MW at 620V. From Fig. 22 (a), the peak value of the line-to-line input voltage of WTG is 877V. From Fig. 22 (c), the peak value of the line-to-line current is 2000A. The system power factor is unity as per Table. 1. The Root-Mean-Square values of the input voltages and currents are given by Eq. (34) and Eq. (35):

$$V_{RMS} = \frac{V_{pk}}{\sqrt{2}} \quad (34)$$

$$V_{RMS} = \frac{877}{\sqrt{2}}$$

$$V_{RMS} = 620V$$

$$I_{RMS} = \frac{I_{pk}}{\sqrt{2}} \quad (35)$$

$$I_{RMS} = \frac{2000}{\sqrt{2}}$$

$$I_{RMS} = 1414.21A$$

The average power delivered by WTG can be computed using (36):

$$P_{avg} = \sqrt{3}V_{RMS}I_{RMS}\cos\theta \quad (36)$$

$$P_{avg} = \sqrt{3} \times 620 \times 1414.21 \times 1$$

$$P_{avg} = 1.5MW$$

Hence, the average power delivered to the system by the WTG is as per the data given in Table.1. From Fig. 22 (a), the peak value of the line-to-line input voltage of VSI is 877V. From Fig. 22 (c), the peak value of the line-to-line current is 2000A. The system power factor is unity as per Table. 1.

The Root-Mean-Square values of the grid voltage and current are calculated by Eq. (34) and Eq. (35) as follows:

$$V_{RMS} = \frac{877}{\sqrt{2}}$$

$$V_{RMS} = 620V$$

$$I_{RMS} = \frac{2000}{\sqrt{2}}$$

$$I_{RMS} = 1414.21A$$

Similarly, the average power delivered by WTG can be computed using (36):

$$P_{avg} = \sqrt{3} \times 620 \times 1414.21 \times 1$$

$$P_{avg} = 1.5\text{MW}$$

Hence, the average power delivered to the grid by VSI is also as per the data given in Table.

3.2 Simulation Results of the Proposed System at Variable Wind Speed

In this section, all stages of the proposed system are simulated under varying wind speed to analyze the behavior of the system whether all parts of the WECS are able to gain their steady-state value after a short period despite the disturbances in wind speed. Fig. 25 gives the wind profile whereby the wind speed is initially normal at 3m/s for an instant of 0.1s then falls to 1m/s for the next 0.2s. Later on, an increase is seen in the wind speed at 0.3s onwards where it rises to 5m/s.

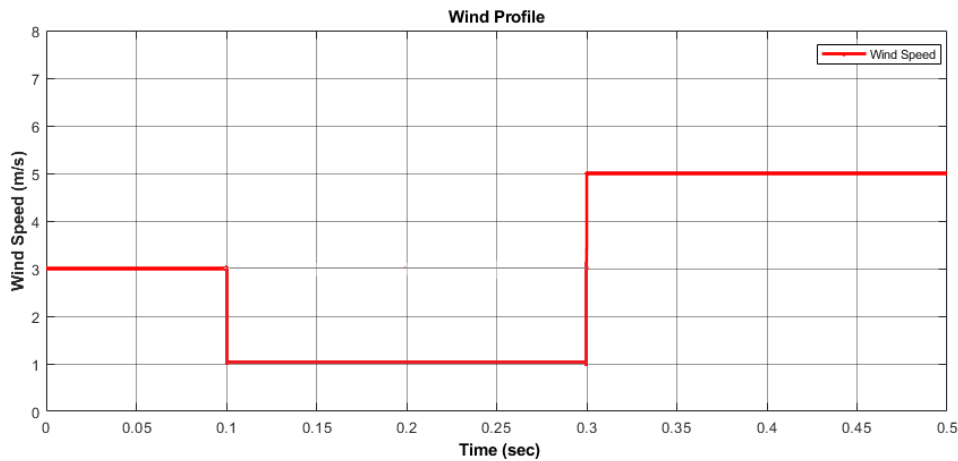


Fig. 25 Wind profile

As it is seen in Fig. 26, the WTG output voltage undergoes small variations as per wind speed variations. At 0.1s, the the peak to peak voltage slightly drops to 850V. Also, at 0.3s it rises to 900V. However, due to DQ-PLL control, WTG voltage reaches steady-state value after 0.05s and continues to remain at 877V peak to peak onwards.

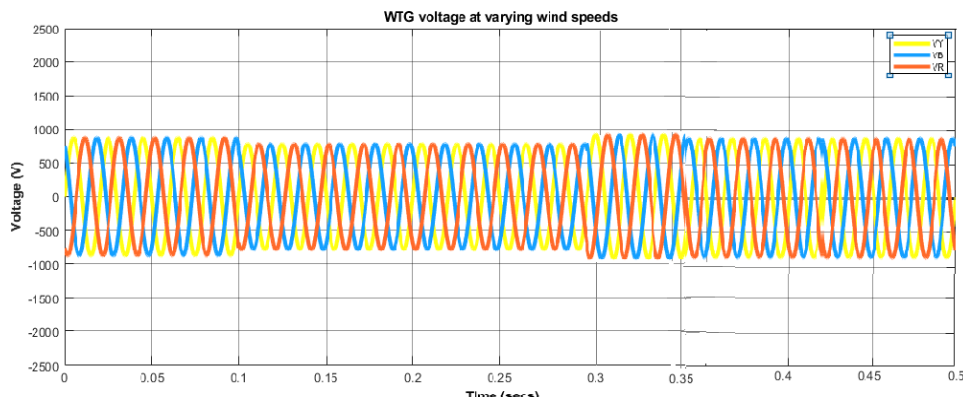


Fig. 26 WTG voltage at varying wind speeds

Fig. 27 gives the WTG current at fluctuating wind speed. At 0.1s, the the peak to peak current slightly falls, then at 0.3s it rises. However, due to DQ-PLL control, WTG current stablizes within 0.05s.

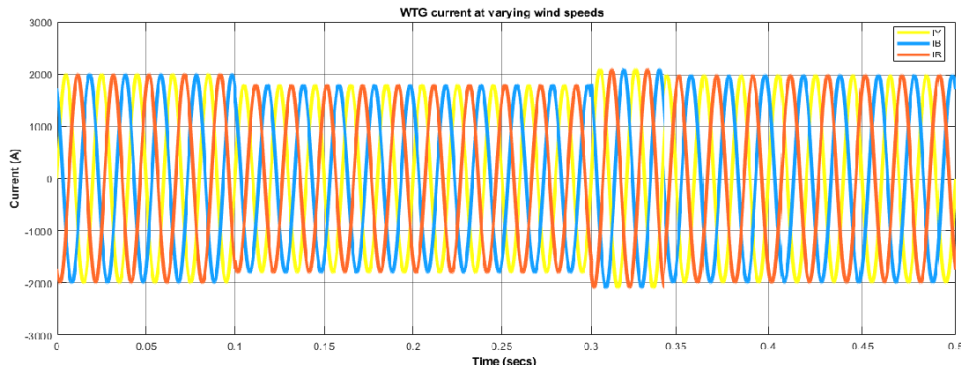


Fig. 27: WTG current at varying wind speeds

Fig. 28 gives the WTG power generated at fluctuating wind speed. Upto 0.1s, the average generated power as calculated in section 11.2.1 is 1.5MW. It undergoes a small fall and rise at 0.1s and 0.3s respectively, but at 0.35s it achieves equilibrium and generates rated power.

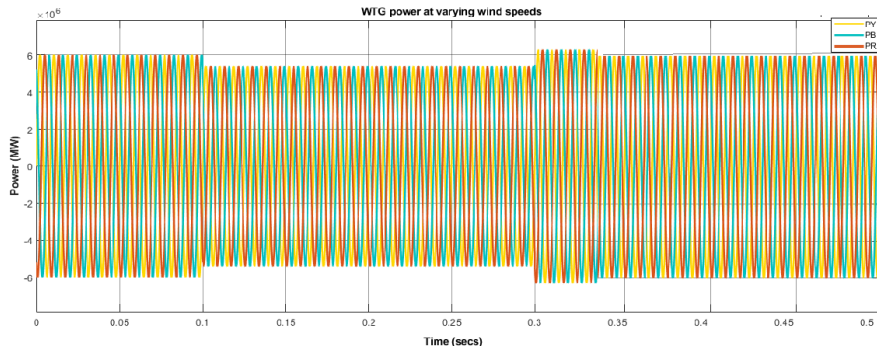


Fig. 28: WTG power at varying wind speeds

As seen in Fig. 29, the input voltage of Cuk converter undergoes variations as per changes in wind speed given in Fig. 25. However, due to the robustness of the sliding mode control the converter output voltage is able to quickly gain equilibrium by shifting to 600V at 0.1s and 0.3s followed by negligible undershoots and overshoots at respective instants.

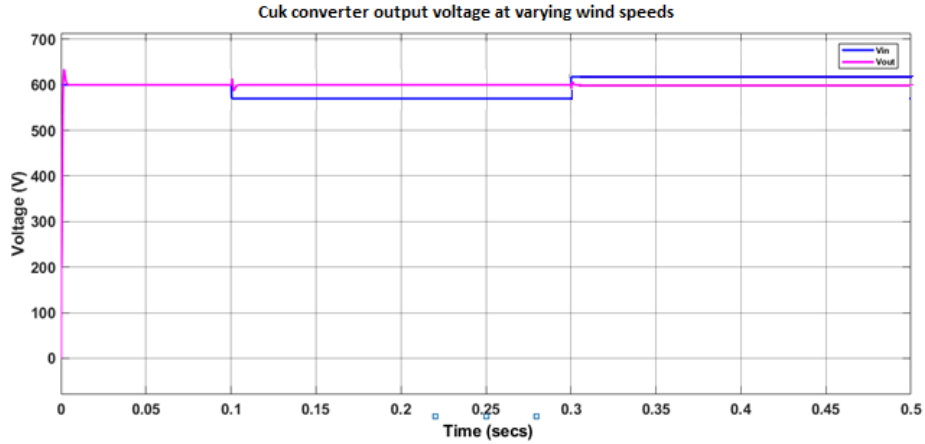


Fig. 29: Cuk converter input and output voltages at varying wind speeds

Fig. 30 (a), (b) and (c) show the converter currents at varying wind speeds. It is seen that all currents gain steady state in a very small interval of time with small spikes at moments of variations in wind speed.

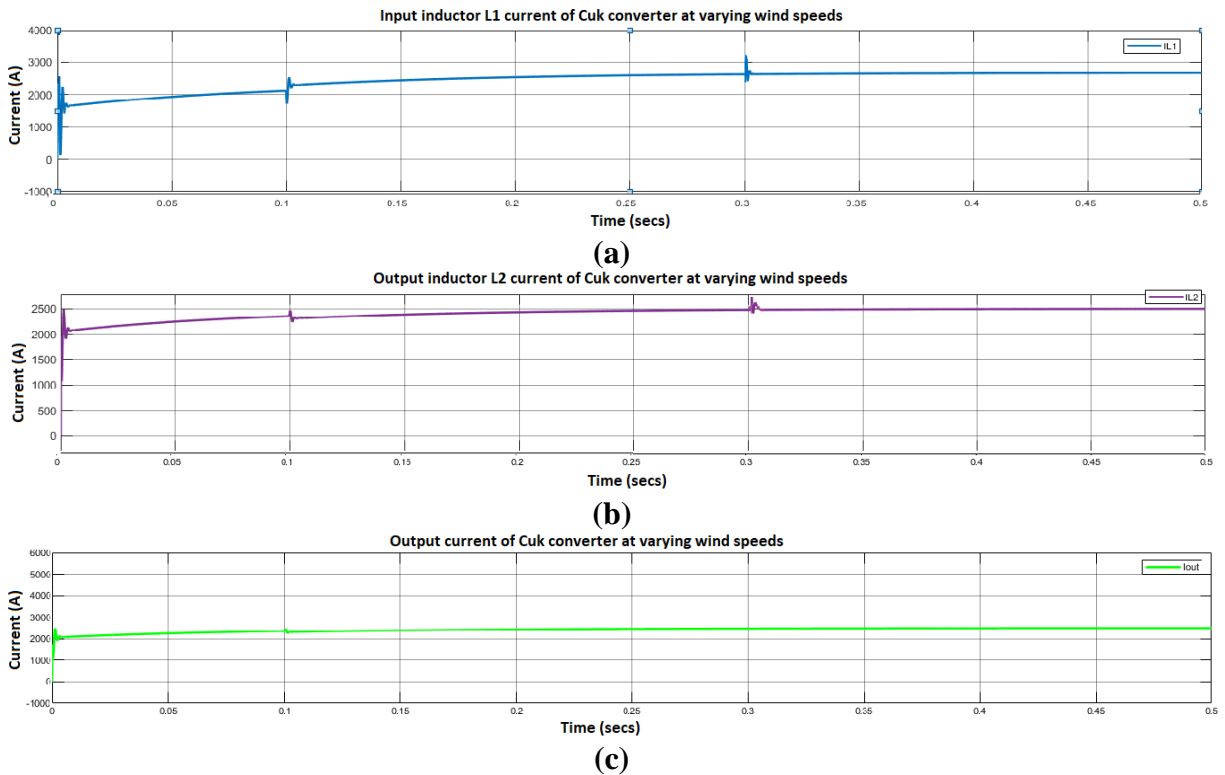


Fig. 30: (a) Inductor L1 current at variable wind speed (b) Inductor L2 current at variable wind speed (c) Output current at variable wind speed

Fig. 31 (a) and (b) show th power input and output of Cuk converer at changing wind speeds. It is seen that both attain steady state in a very small interval of time with small spikes at moments of variations in wind speed.

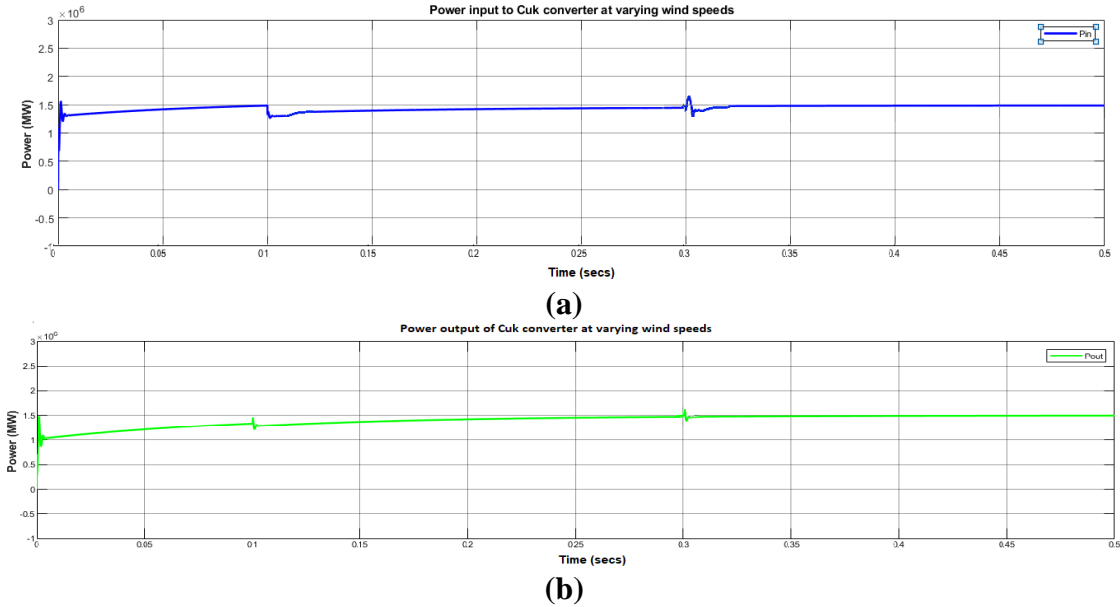


Fig. 31: (a) Power input of Cuk converter at varying wind speeds (b) Power output of Cuk converter at varying wind speeds

Fig. 32(a), (b) and (c) show the output voltage, current, and power of the VSI respectively. In other words, they show the grid voltage, grid current and power delivered to the grid at changing wind speeds. It is clear from Fig. 32 (a), (b) and (c) that after an interval of 0.05s at 0.3s, the waveforms reach their rated values.

1. Conclusion

Due to the stochastic nature of wind speed, the power generated by wind turbines at a particular voltage is of poor quality given that a suitable controller is not there to tackle this issue. This problem of votage regulation is widely handeled with MPPT conrolled DC-DC converters. In this article, an SMC Cuk converter was employed to improve voltage regulation of a WECS model based on real-time data. The heart of this work was the modeling of one out of 33 WTG units of Sachal Wind Farm, Jhimpir on MATLAB Simulink. Initially, the model was simulated at rated wind speed 3m/s. The simulation results of each stage were exactly same as were in the system data. The model was simulated under varying wind speed. In the simulation results of the WTG and VSI, the voltages, currents and powers attained steady state in 0.05s. In th simulation results

of the SMC Cuk converter, the voltage, currents and powers attained steady state in a very short period of time with minimum undershoots and overshoots.

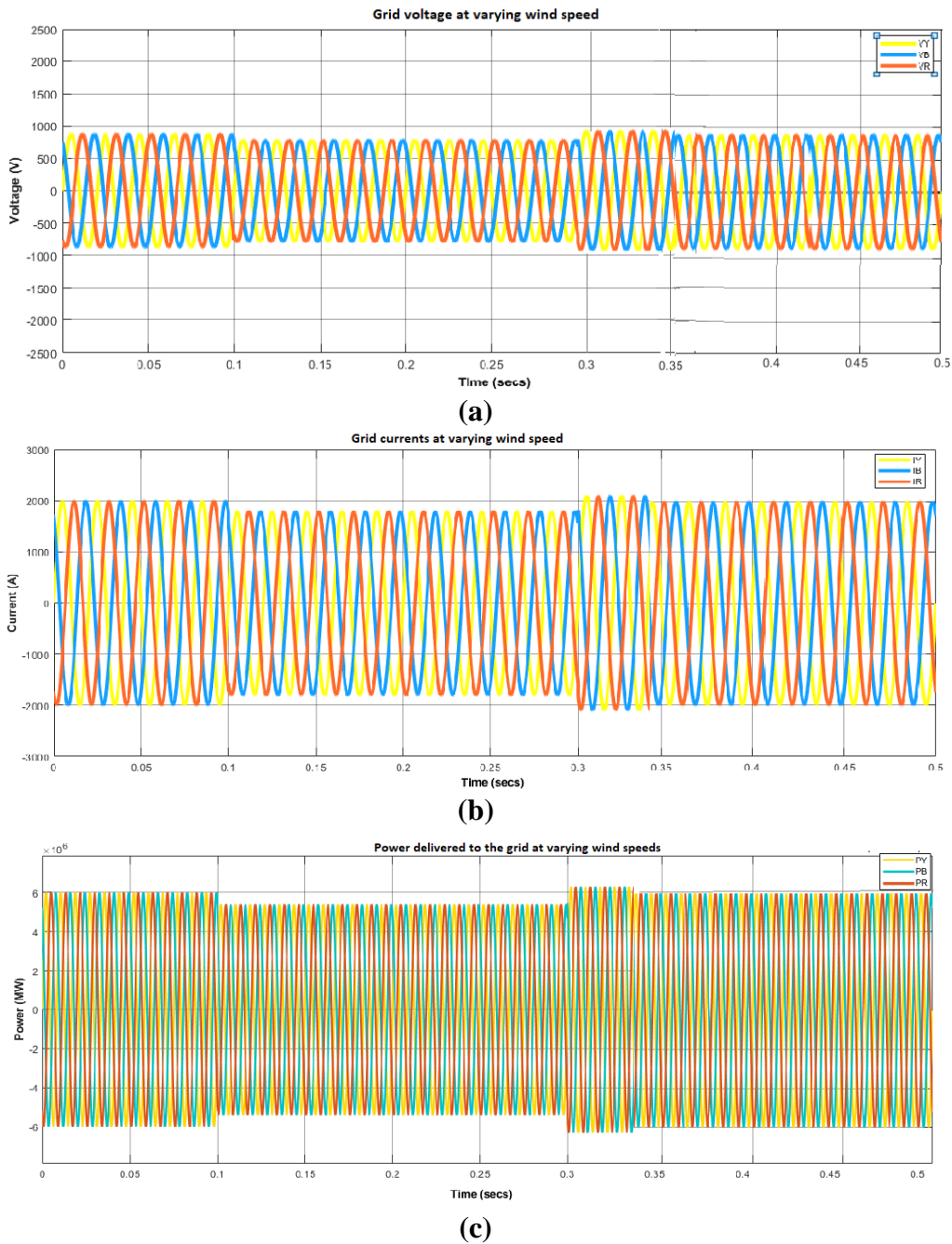


Fig. 32: (a) Grid voltage at changing wind speeds (b) Grid currents at changing wind speeds (c) Power delivered to the grid

References

[1] S. Haghighi et al, "Developing more efficient wind turbines: A survey of control challenges and opportunities.," *IEEE Industrial Electronics Magazine*, vol. 14(4), no. pp.53-6, 2020.

- [2] S. Shi and K. Lo, "An overview of wind energy development and associated power system reliability evaluation methods.," in *48th International Universities' Power Engineering Conference (UPEC)*, 2013.
- [3] M.S. Al-Soud and Q.H. Alsafasfeh, "Economical evaluation for various renewable energy products in Jordan". In *The Sixth International Renewable Energy Congress IREC2015*, Sousse, Tunisia, 24-26 March 2015, pp. 1-4.
- [4] S. Shoaib et al, "Holistic and Scientific Perspectives of Energy Sector in Pakistan: Progression, Challenges and Opportunities", *IEEE Access*, 8, pp.227232-227246, 2020.
- [5] Wikipedia. (2023, August.) Lists of power stations in Pakistan [Online]. Available: https://en.wikipedia.org/wiki/List_of_power_stations_in_Pakistan .[Accesses: Sept.5, 2023].
- [6] S. Samreen and W. Rashid, "A review of the wind power developments in Pakistan", *Renewable and Sustainable Energy Reviews*, 57, pp.351-361, 2016.
- [7] S. Bhim and K.K. Gaurav, "Solid-state voltage and frequency controller for a stand-alone wind power generating system," *IEEE Transactions on Power Electronics*, vol. 23, no. 3, pp. 1170–1177, 2008.
- [8] J. Bhavna et al, "Flexible mode control of grid-connected wind energy conversion system using wavelet", *Journal of Energy*, Vol 2015, Article ID 152898, 2015.
- [9] D. N. Ronny et al, "Design and implemented buck-boost converter based fuzzy logic control on wind power plant", *International Journal of Mechanical and Mechatronics Engineering IJMME-IJENS*, Vol:20 No:01, 2020.
- [10] K. Saurabh, K. Vijayakumar and K. Rajvir, "Unified controller for bidmodal operation of Cuk converter assisted SEIG-based DC nanogrid", *IEEE Systems Journal*, Vol 15, 2, 2020.
- [11] A. J. Samuel, "Novel PID-SMC controller for Cuk converter in permanent magnet synchronous wind generator with MPPT control", in *2022 IEEE ANDESCON conference*, IEEE, Barranquilla, Colombia, 16-19 November 2022,
- [12] T. Porselvi and M. Ranganath, "The PMSG based Wind Energy Conversion System with CUK Converter and CHB MLI with a Single DC Input", *International Energy Journal*, 14, 43-56, 2014.
- [13] R. Erickson and D. Maksimovic, *Fundamentals of Power Electronics.*, New York:Kluwer Academic/Plenum Publishers, 2004.
- [14] M. H. Rashid, *Power Electronics: Circuits, Devices and Applications*, 2010

- [15] K. Saurabh, K. Rajat and S. Navdeep, "Performance of closed loop SEPIC converter with DC-DC converter for solar energy system", in *IEEE 4th International Conference on Power, Control and Embedded Systems, ICPCES*, 2017, MNNIT Allahabad, 9-11 March, 2017, pp. 1-6.
- [16] H. Yang et al, "Average-value model of modular multilevel converters considering capacitor voltage ripple", *IEEE Transactions on Power Delivery*, 2016, 32(2), pp.723-732.
- [17] D. T. Sepsi, J. Hamar, and R.K. Járđán, "Sliding mode agent-based control of parallel buck converters", In *Proceedings of 14th International Power Electronics and Motion Control Conference EPE-PEMC*, September 2010, IEEE, (pp. S13-20).
- [18] S. Sharma and C. Dixit, 2020, "Design of PID controller for dc to dc converter to improve the voltage profile", Galgotias University, *Manufacturing Engineering*. s.l.:s.n.
- [19] Circutor, n.d. *Circutor*. [Online]. Available at: docs.circutor.com/docs/M98121701-03.pdf [Accessed 10 2022].
- [20] G. Majic, M. Despalatovic, and B. Terzic, "LCL filter design method for grid- connected PWM-VSC", *Journal of Electrical Engineering and Technology*, 12(5), pp.1945-1954, 2017.
- [21] Martinek et al, "Design of a measuring system for electricity quality monitoring within the smart street lighting test polygon: Pilot study on adaptive current control strategy for three-phase shunt active power filters". *Sensors*, 20(6), p.1718. 2020.
- [22] P. Rodriguez, and N.B. Lai, "Grid-following and grid-forming PV and wind turbines", In *Control of Power Electronic Converters and Systems* (pp. 499-521).Academic Press, 2021.
- [23] E. Kabalcı, A. Boyar, and Y. Kabalcı, "Pulse width modulation and control methods for multilevel inverters". In *Multilevel Inverters* (pp. 1-33). Academic Press, 2021
- [24] K.R. Sekhar, M.A Chaudhari and T.D.C. Busarello, "A PLL-less Vector Control technique for the single-phase Grid connected inverters", *International Journal of Electrical Power & Energy Systems*, 142, p.108353, 2022.
- [25] L. Yahui et al, "Improved PR Control Strategy for an LCL Three-Phase Grid-Connected Inverter Based on Active Damping", *Applied Sciences*, 11(7), p.3170, 2021
- [26] N. Hamrouni, M. Jraidi, and A. Chérif, "New method of current control for LCL-interfaced grid-connected three phase voltage source inverter", *Journal of Renewable Energies*, 13(1), pp.71-84, 2010.